Journal of Electrostatics 69 (2011) 401–409

Contents lists available at ScienceDirect

Journal of Electrostatics

journal homepage: www.elsevier.com/locate/elstat

Electric potential decay on polyethylene: Role of atmospheric water on electric charge build-up and dissipation

Thiago Augusto de Lima Burgo [a], Camila Alves Rezende [a], Sérgio Bertazzo [a], André Galembeck [b], Fernando Galembeck [a,*]

[a] Institute of Chemistry, University of Campinas – Unicamp, PO Box 6154, CEP 13084-971, Campinas, SP, Brazil
[b] Departamento de Química Fundamental, Universidade Federal de Pernambuco, Av. Prof. Luiz Freire, CDU, CEP 50670-901, Recife, PE, Brazil

ARTICLE INFO

Article history:
Received 14 December 2010
Received in revised form
19 April 2011
Accepted 9 May 2011
Available online 31 May 2011

Keywords:
Charge dissipation
Adsorption
Polyethylene
Kelvin probe
Kelvin force microscopy
Water

ABSTRACT

Electrostatic potential decay on corona-charged low-density polyethylene (LDPE) was recorded as a function of position and time, using a macroscopic scanning electrode and also Kelvin force microscopy. Potential decays independently in adjacent sample areas until reaching equilibrium at negative values (4.6 ± 0.7 V), irrespective of the initial potential signal. Other observations already described in literature were confirmed: negative potential decays slower than positive potential and the relative humidity has a large effect on the dissipation rates. These results are discussed considering ion exchange associated to adsorption and desorption of water clusters at the solid–gas interface.

1. Introduction

Electrostatics has been studied for centuries and it is now related to several applications such as electrets [1,2], copying machines and laser printers [3]. Important industrial processes are based on electrostatics, for instance, electrostatic painting [4], electrospraying and electrospinning [5]. While fundamental concepts on this topic are well established for metals and semiconductors, knowledge on the electrification of dielectrics is rather empiric and important questions remain unanswered [3].

The electric potential distribution on the surface of any insulating polymer, glass or ceramic is usually neglected, though it should affect electric, optical, mechanical, chemical, adhesive and permeation properties of the material. Even though these materials are usually considered as electroneutral, they may present considerable electric heterogeneity, as observed on electric force and electric potential microscopy surface maps obtained by scanning probe techniques [6–10]. Dielectric solids with well-defined composition, either polymers, metal oxides or silicates, often present excess electrostatic charge that may persist for considerable amounts of time [11–13].

An important question related to electric phenomena on dielectrics or insulators is the identity of charge carrier species [3,14]. Detailed examination of the literature shows that their detection and speciation have seldom been achieved, leading to serious difficulties to explain the behavior of electrified insulators. In the case of polymer latexes and their cast films, charge distribution was correlated to spatial separation of cations and anions remaining from synthesis, as determined by analytical transmission microscopy [8–10]. However, for common thermoplastics the speciation of charge carriers has not yet been accomplished [15], although it is now acknowledged in the literature that dielectrics have peculiar charge mobility mechanisms, distinct from conductors [16–19].

Important new evidence for charge carrier speciation in insulators is currently appearing: partition of hydroxide ions derived from adsorbed water is emphasized by Whitesides and collaborators [20–22] while Liu and Bard [23] presented evidence for excess electrons on tribochemically charged polytetrafluoroethylene. It has also been suggested that ions on the material surfaces may originate from the atmosphere but this is not a widespread idea. Even though, some experimental findings are well established. It is clear that the surrounding atmosphere is fundamental for charge build-up (either by triboelectrification or induction) and dissipation on dielectrics [24]. Hogue *et al.* demonstrated the effect of atmospheric pressure [16–18] and other authors showed the

* Corresponding author. Tel.: +55 19 35213080; fax: +55 19 35212906.
E-mail address: fernagal@iqm.unicamp.br (F. Galembeck).

0304-3886/$ – see front matter © 2011 Elsevier B.V. All rights reserved.
doi:10.1016/j.elstat.2011.05.005

importance of atmospheric humidity [25–28]. For instance, glass beads in a fluidized bed do not show any charging at RH > 40% but they are strongly charged at lower RH [25] and the stationary charge acquired by alumina under pneumatic flow is lower at higher humidity [26]. Several reports show that surface conductivity of dielectrics increases with atmospheric humidity and this is assigned to absorbed water [29–31]. Other papers showed that fluidization velocity of fluidized bed has strong influence on the electrification of insulating particles [25,32].

Recent experimental results from this group on electrostatic charging of silica [33,34], cellulose and glass [35] surfaces, Stöber silica and aluminum phosphate [36] particles, mica coated with surfactant [37] and a number of isolated metals [38] were interpreted using the following hypothesis: surface charges in these insulating materials are ions formed by dissociation of adsorbed water molecules that accumulate under the local electrostatic potential. Atmospheric water is thus the source and sink of ions in insulators, thus contributing to potential build-up and dissipation [39].

The same model is used here to interpret the results obtained using low-density polyethylene samples, charged with corona ions produced by a piezoelectric gun. Electrostatic potentials on the LDPE pieces were measured as a function of time, using a scanning system that yielded a large number of electrostatic potential measurements on many samples during potential dissipation. By varying the environmental humidity during the measurements, it was possible to evaluate the effect of relative humidity on the rate of potential decay. Kelvin Force Microscopy (KFM) and Electric Force Microscopy (EFM) images were also obtained for these samples yielding electric potential maps at the nanometer scale.

2. Experimental

2.1. Polyethylene samples

Samples were prepared by cutting injected LDPE (Dow) slabs into small pieces (30 mm × 12 mm × 3 mm) using a sharp blade. Two sample sets were used: samples from the first set were gently wiped with a sponge soaked in commercial detergent, and rinsed thoroughly with distilled water, then deionized water, and finally dried at room temperature prior to use. Most results presented in this work were obtained using these samples, except where mentioned otherwise. The other set is formed by samples washed in different ways: (a) with boiling acetone in a Soxhlet apparatus for 60 min; (b) soaking polyethylene pieces in aqueous NaOH solution (0.01 mol L^{-1}) for 30 min, then rinsing abundantly with deionized water; (c) soaking in aqueous HCl solution (0.01 mol L^{-1}) for 30 min, then sonicating for 36 min and rinsing with deionized water and (d) washing with detergent, as described for the first set of samples. In every case, rinsed samples were immediately set up in the aluminum sample holder, dried in an oven for 1 h at 50 °C and placed in the apparatus sample holder.

2.2. Electrostatic potential measurements

The scanning apparatus for potential measurements and the controlling software were built by Optron (Campinas) following the authors' design shown in Fig. 1(a). It consists in an aluminum plate (4 mm thick) as a sample holder and in a disc shaped 5 mm-diameter Kelvin electrode connected to a Trek model 320 C voltmeter. This system can measure potentials in the −200 to +200 V range and a mechanical arm moves in the *x*–*y* plane, allowing the electrode to scan over the samples. Sample holder plate is always connected to the ground and it has 12 relief positions, where samples are fitted, flush with the sample holder. The whole assembly is placed inside a metal box and enclosed by a polyethylene plastic bag, which helps to control the environmental humidity.

Humidity inside the box was controlled by changing the flow of two merging N_2 currents: one is dry and the other is water-saturated, produced by bubbling N_2 through distilled water. Temperature was controlled by an air conditioning system that kept the room temperature at 23 ± 2 °C. Both the temperature and the humidity inside the box were continuously monitored using a digital thermohygrometer (Minipa MTH-1380).

Prior to corona charging, samples were maintained inside the metallic box under controlled temperature and humidity for 24 h. Samples were charged with a Zerostat piezoelectric antistatic gun (Aldrich) whose tip was kept at an approximate distance of 10 cm from the samples. Low density polyethylene pieces were charged in pairs so that each row in the sample holder plate had two pairs of samples rendered negative (1 and 2, 5 and 6) and two pairs rendered positive (3 and 4, 7 and 8) as indicated by positive and negative symbols in Fig. 1(b).

Electrostatic potential scans started immediately after all samples had been charged (that took *ca.* 2 min), and spatial resolution (5 × 5 mm) is limited by the Kelvin electrode dimensions. Time allowed for the electrometer equilibration on each point was 8 s. The overall sample scans were started every 4 h during approximately two weeks at 3, 20, 40 or 60% RH.

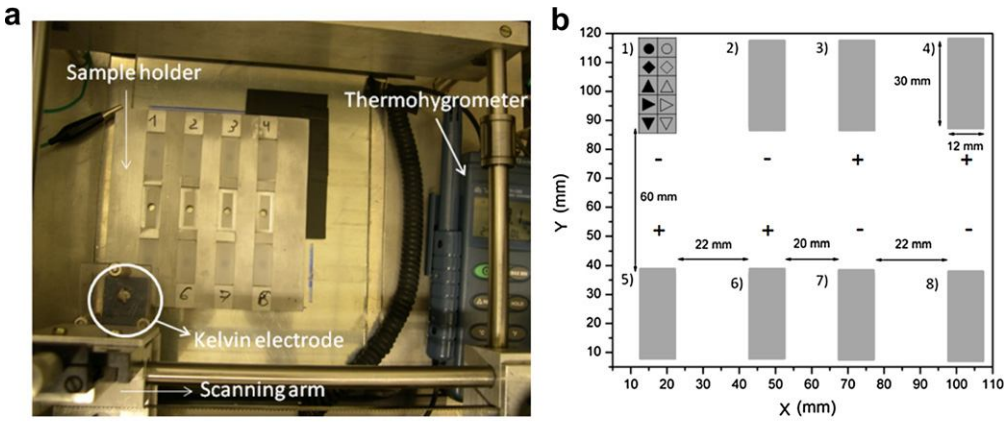

Fig. 1. (a) Picture of the scanning apparatus for electrostatic potential measurements and (b) schematic representation of the polyethylene samples mounted on the aluminum sample holder. The + and − signs indicate samples with initial positive or negative excess charges. (Symbols in block 1) identify the sampling areas on each sample (see Fig. 3).

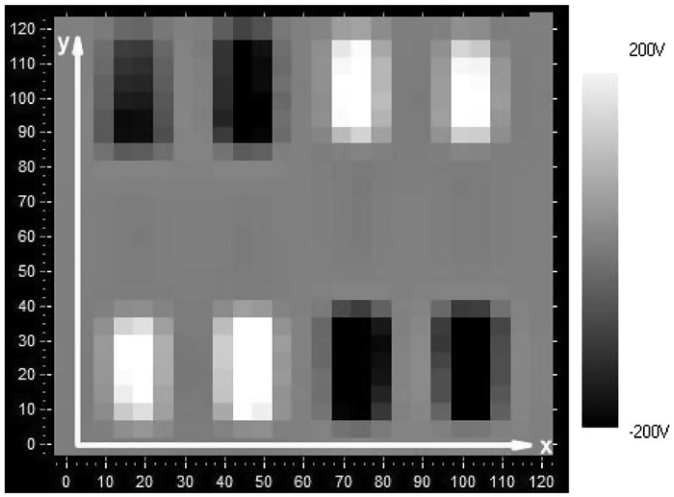

Fig. 2. Electrostatic potential map of eight polyethylene samples under 40% RH, immediately after the samples were corona-charged.

2.3. Kelvin force probe microscopy (KFM) and electric force microscopy (EFM)

Samples for KFM and EFM measurements were cut into squared small pieces (~5 mm side) and imaged in non-contact mode. For KFM, a scanning probe microscope Shimadzu SPM-9600 was used, with a silicon tip Nanoworld EFM-20 (resonance frequency = 79 kHz and force constant = 2.6 N/m). KFM scanning system is enclosed within an environmental chamber to control temperature (25 ± 1 °C) and relative humidity during electric potential scanning.

EFM images were obtained in a Discoverer TMX 2010 microscope (TopoMetrix), using Pt-coated Si probes (Veeco) with 60–100 kHz resonance frequency and force constant within the 1–5 N/m range.

2.4. Evaluation of charge surface density

Evaluation of excess surface charge density on the samples follows the procedure described in a previous paper [33]. In brief, each pixel in the surface map is a square with 5 mm sides and the image is a 255×255 pixel matrix where virtual charges are placed. The electrostatic potential (V_T) measured in a point of a plane 1 mm away from the matrix plane is generated by all charges (q_i) weighted by the distance r (from the charge to the measuring point), and can be calculated, using a C++ code for Eq. (1) [40]. The number of excess charges per pixel is adjusted by trial and error, until the calculated and measured potentials match, within experimental error.

$$V_T = \sum_{i=1}^{n} V = \frac{1}{4\pi\varepsilon_0} \sum_{i=1}^{n} \frac{q_i}{r_i} \tag{1}$$

3. Results

A typical electrostatic map is presented in Fig. 2, showing eight polyethylene samples after corona charging at 40% RH. Black areas represent negative potentials, while white or clear gray areas are positive, according to the potential scale on the right side of the

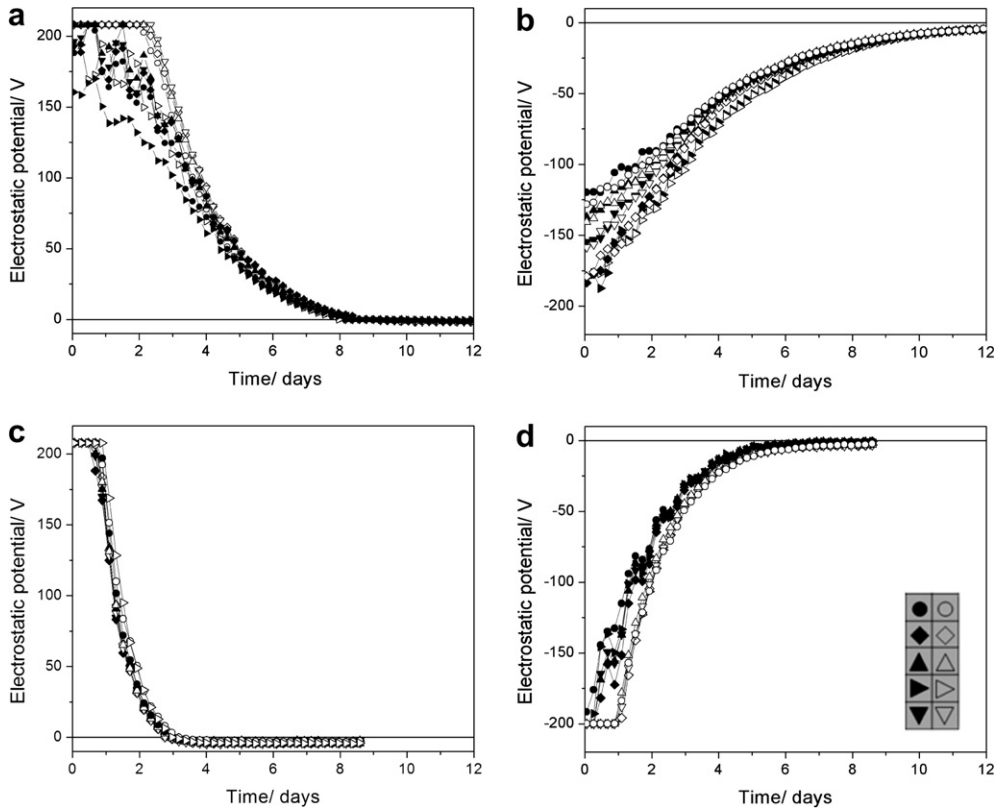

Fig. 3. Representative plots of electric potential decay as a function of time on polyethylene samples, showing 10 curves for each sample: (a) and (b) at 3% RH; (c) and (d) at 60% RH. Note that (a) and (c) are initially positive and (b) and (d) are negative. The sampling area for each curve is indicated by symbols in Fig. 1 and insert in Fig. 3(d). The voltmeter measurement range is within ±200 V.

image. The metal sample holder appears as a gray background on the map at 0 V. Similar maps were obtained at 3, 20 and 60% RH.

Each polyethylene sample contains ten 5 × 5 mm^2 (Fig. 1(b)) pixels and the potentials determined on these pixels can be plotted as a function of time, yielding curves of potential decay for distinct points on the sample, as shown in Fig. 3. Duplicates for polyethylene samples under all the relative humidity values measured are also in the Supplementary data. The overall decay patterns are rather uniform but some curves clearly deviate from the others, even though they are measured on the same sample. Initial potential for some curves in Fig. 3 are in excess of the electrode detection limit (±200 V) producing flat curve sections at *ca.* ±200 V that are just artifacts. Curves in Fig. 3 can be averaged considering the ten points measured on each sample and the average curves are given in Fig. 4.

Electrostatic potential maps also contain information on the metal sample holder surface. Fig. 5 shows electric potential plots (under 3% RH) for two points (A and D) on the samples together with potentials measured on two adjacent points (B and C) on the metallic sample holder. The surface potential on aluminum areas adjacent to electrified LDPE has signal opposite to LDPE, as expected due to induction in the metal. It shows that LDPE charge decay receives little contribution from the surface conduction, since potential gradients are not evident on the charged surfaces. Far from LDPE samples, the potential on the sample holder surface is zero.

Two parameters were extracted from each potential *vs.* time experimental curve: the final constant electric potential at each point (equilibrium potential) and the half-life of potential decay, defined as the time required to halve the maximum potential attained by the sample. In samples with maximum potential higher than the electrode measuring limit, an extrapolation to $t = 0$ was done using Eq. (2). Experimental data can be fitted by exponential curves described by Eq. (2), where V is the electric potential, V_0 is a constant, t is the time, and τ is the time constant.

$$V = V_0 e^{t/\tau} \tag{2}$$

Figs. 6–8 contain information on the half-lives for potential dissipation and equilibrium potential for LDPE samples under variable relative humidity. In Fig. 6, significant differences appear between half-lives for distinct points on the samples, considering the timescale from 1 to 200 h on the right side of the image. Electrostatic potential dissipation rates are generally slower at a 3% relative humidity than at higher RH values (20%, 40% and 60%) but the values also vary with the potential sign. Negative potentials generally decay at a slower rate than positive ones, which is especially noticeable on the maps for relative humidities higher than 20%.

Besides, there is a difference between positive and negative charge decay, considering the influence of relative humidity. For positive potentials, half-lives are a few times longer under 3% RH than under 60% RH, while the average half-life for dissipation of negative potentials is only *ca.* 2 times longer at 3% RH than at 60% RH. The stronger influence of the relative humidity on the dissipation rates of electric potential in positively charged samples is in agreement with earlier results by Baum *et al.* [41], who showed that the decay rate for negatively charged polyethylene films is only slightly affected by atmospheric humidity, whereas in positively charged films decay rates decrease as humidity falls.

The effect of the relative humidity on the half-lives of electric potential dissipation can be also noted on the data presented in Fig. 7, which shows the average half-lives for ten areas on each sample (considering also the duplicates) as a function of the RH. Even though the error bars are rather important, these graphs

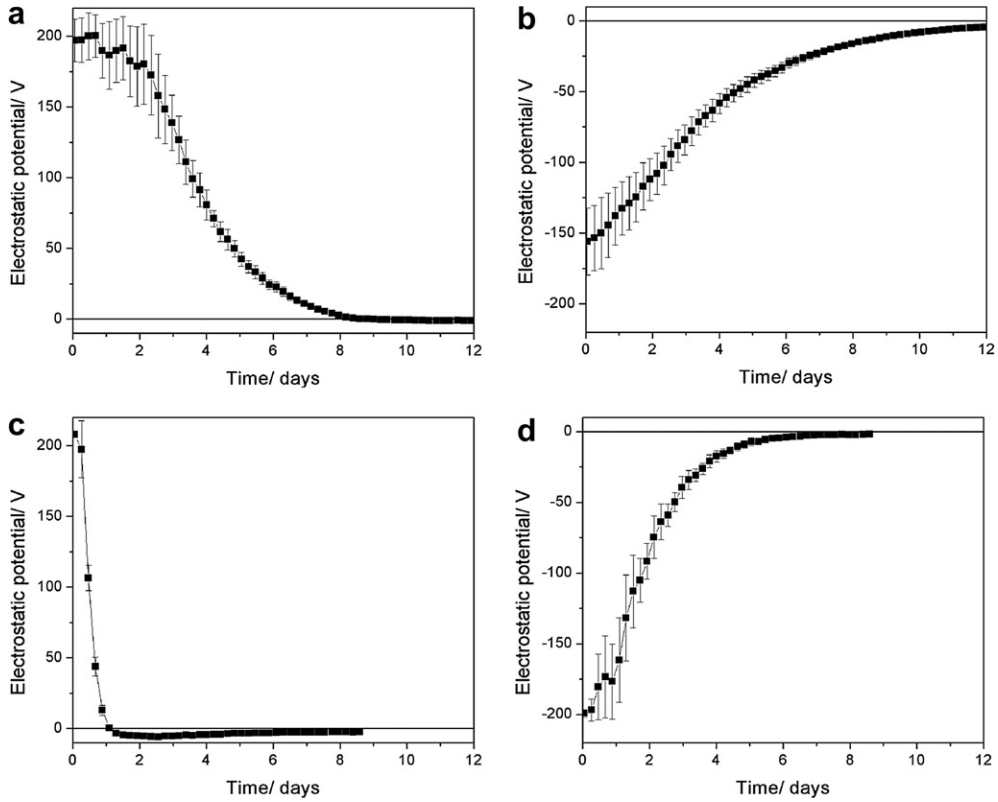

Fig. 4. Electric potential decay as a function of time on polyethylene samples: (a) and (b) at 3% RH; (c) and (d) at 60% RH. Averaged values with error bars are obtained from the 10 curves for each sample shown in Fig. 3. Note that (a) and (c) are initially positive and (b) and (d) are negative.

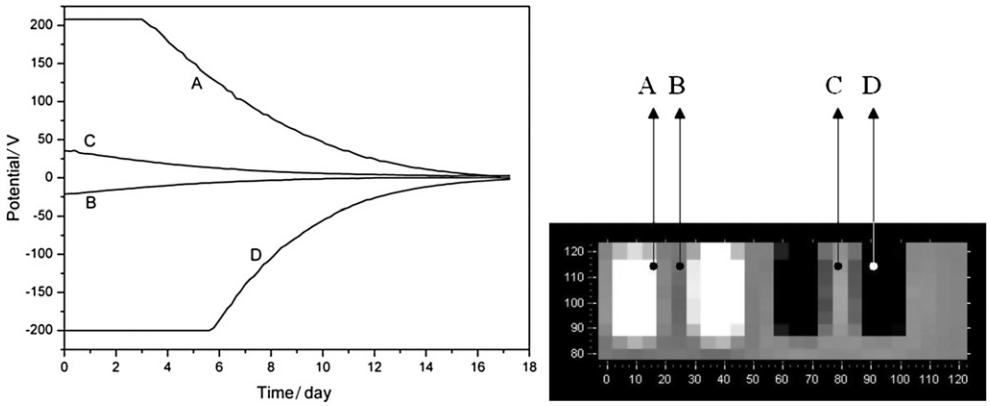

Fig. 5. Electric potential decay for two pixels on the LDPE samples (A and D) and on the aluminum sample holder (B and C) at 3% RH. Pixel positions corresponding to points A–D are shown on the map at the right side of the image.

confirm the large RH effect on electric potential dissipation: (i) dissipation rates increase with the humidity; (ii) negative charges are generally more slowly dissipated than the positive ones and (iii) the increase in relative humidity from 3 to 60% RH produces a more significant effect on the dissipation rate for positive samples.

It is remarkable that all the potential *vs.* time curves like those shown in Fig. 3 and on the Supplementary Material converge to low negative values. This suggests that there is an equilibrium potential for LDPE, under the experimental conditions used in this work. The average equilibrium potential values obtained from 10 areas on each polyethylene sample are presented in Fig. 8. Even considering the error bars, the values are always negative, lying between −0.5 and −4.8 V. The convergence of the sample electrostatic potentials to a narrow range of non-zero values is completely unexpected, considering that polyethylene is a molecular solid that is not supposed to carry excess ionic species.

To better investigate the equilibrium potential behavior, another set of polyethylene samples was carefully washed according to four different procedures: (a) boiling acetone in a Soxhlet extractor; (b) immersion in aqueous NaOH or (c) HCl followed by ultrasonication and (d) gentle wiping in surfactant solution using a sponge and extensive rinsing with deionized water. Right after being removed from the rinsing liquids, samples were laid on the metallic sample holder and dried in an oven at 50 °C.

The electric potential measurements started as soon as the samples were dry (but they were not submitted to corona charging) and continued until the potential values became constant. The equilibrium potential map of the washed samples is presented in

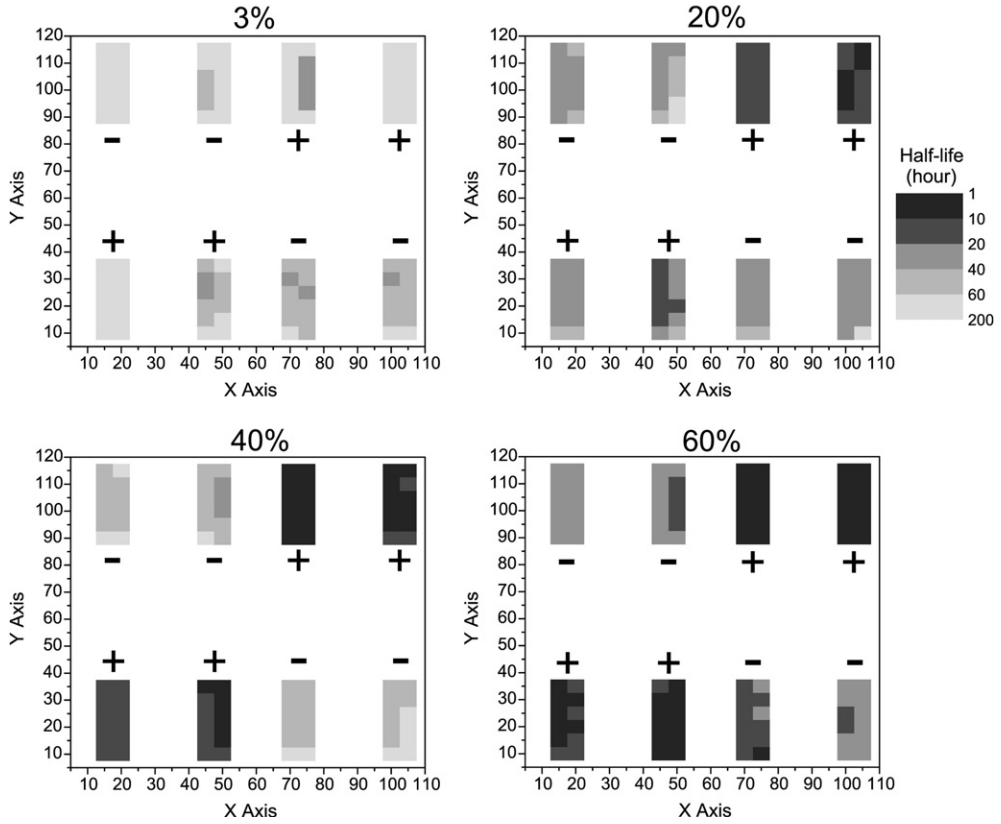

Fig. 6. Maps showing the half-lives of electric potential decay as a function of the position on LDPE pieces under variable relative humidity.

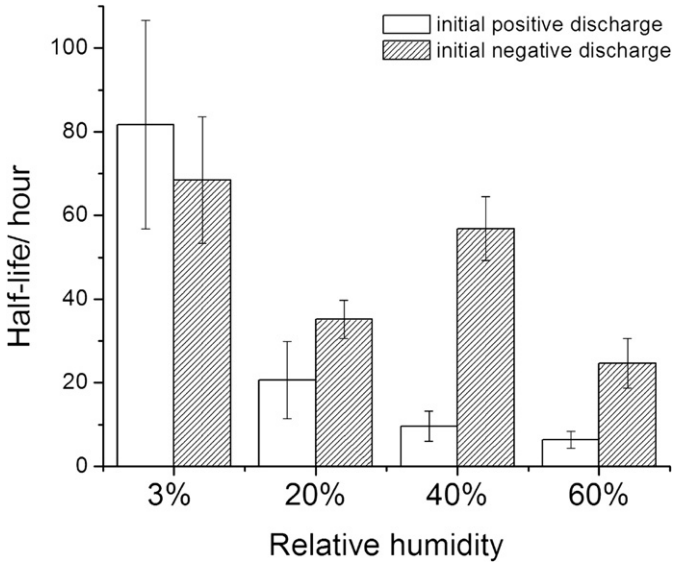

Fig. 7. Average half-life of electric potential dissipation for LDPE pieces positively and negatively charged as a function of the relative humidity.

Fig. 9(a) and the averages of 10 measured equilibrium potentials for each sample at 1% and 60% RH are presented in Fig. 9(b). Equilibrium potentials are negative for all samples washed in different ways and have an average value equal to (-4.6 ± 0.7) V, consistent with the values presented in Fig. 8. This confirms that LDPE has an intrinsic negative equilibrium potential and it can be used to calculate equilibrium excess charge density as described in the experimental procedure. Using the average value (-4.6 ± 0.7) V, average charge density is calculated to be only 0.31 charges/μm^2.

Images by electric force microscopy were obtained on LDPE samples carefully washed with HCl, rinsed and dried under air. Fig. 10(a) shows a relatively flat topography on this sample with variations *ca.* 300 nm height, while the electric force image reveals significant electric heterogeneity on the surface, with coexisting neighboring domains of opposite charge.

Kelvin force microscopy (KFM) images were acquired, showing the electric potentials resulting from excess charges on the surface.

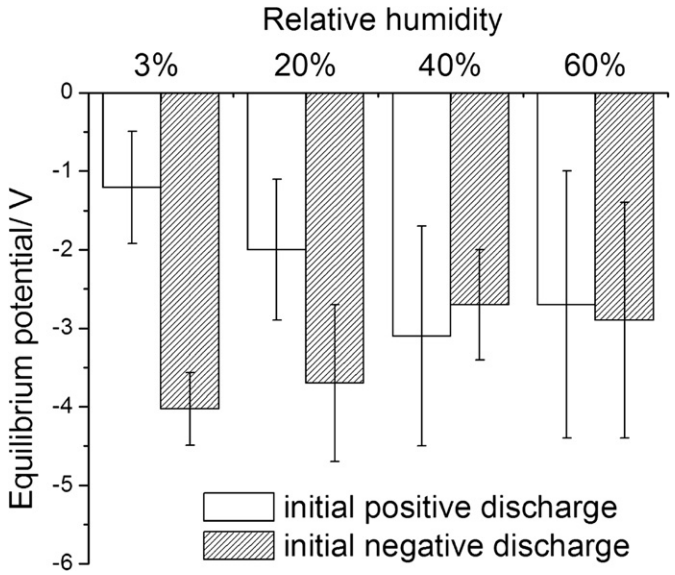

Fig. 8. Average equilibrium potential for each LDPE piece as a function of the relative humidity.

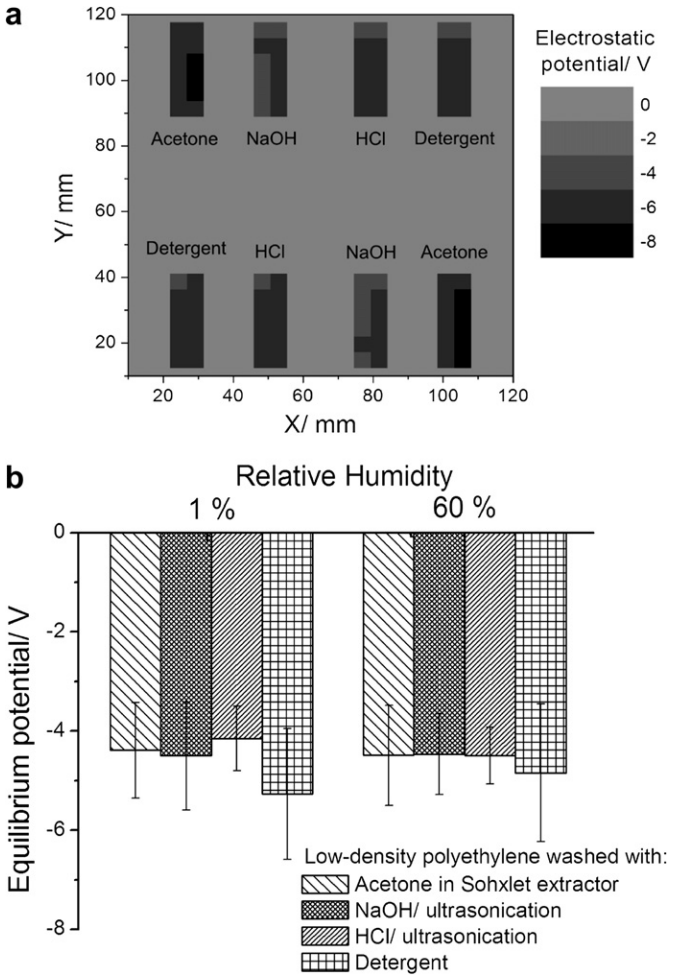

Fig. 9. (a) Equilibrium potential maps of polyethylene samples washed in different ways at 60% RH; (b) averaged equilibrium potentials at 1% and 60% RH.

Samples were also washed with HCl and dried, then equilibrated under air saturated with water vapor and transferred to the microscope environmental chamber at 30% relative humidity. During image scanning, samples were kept under controlled temperature (25 °C) and 30% relative humidity.

The electrostatic potential image presented in Fig. 11(b), together with the corresponding non-contact AFM topography image in Fig. 11(a), show significant contrast, evidencing that the potentials measured using the macroscopic Kelvin electrode arise from the summation of a large number of charge contributions present at a nanoscale. The potential values measured in this area of 6.25 μm^2 are in the negative range, from -7 to -5 V, in good agreement with the macroscopic measurements.

Fig. 11(c) shows the potential variation along three horizontal lines (A–B, C–D and E–F) in the electric potential image, indicated in Fig. 11(b). Potential derivatives with the distance ($\Delta V/\Delta d$) can be calculated in these lines, yielding the electric field component along the *x*-axis, shown in Fig. 11(d). Thus, the surface is electrically rough and large electric fields with spikes reaching the 15–30 MV/m range are calculated, parallel to the surface plane.

4. Discussion

Half-lives of potential decay change significantly from one point to another on polyethylene surfaces and equilibrium potentials also

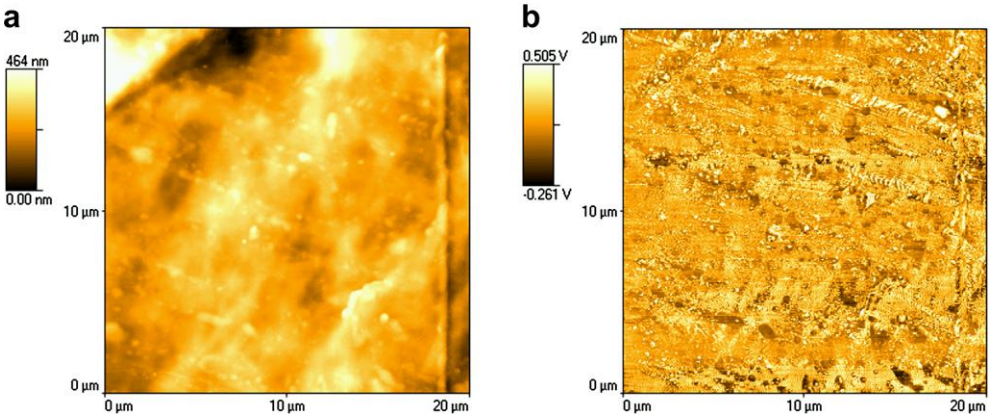

Fig. 10. (a) Topography and (b) electric force images obtained by EFM on LDPE samples washed with HCl.

show some local variations, not only among different LDPE slabs but also within the same slab, down to the nanometer scale. Large surface potential gradients are observed in the images obtained by Kelvin probe force microscopy so that potentials measured macroscopically are the result of a large number of contributions from charged domains. Electric force maps obtained on the same sample also show heterogeneous charge domains due to fixed charges on the surface or beneath it. The electric field component along the *x*-axis can reach relatively high values, close to dielectric strength values [42].

Other experimental results in the literature obtained using other types of polymer charging experiments can be interpreted considering polymer surface heterogeneity, but this is not usually considered or evidenced. Acknowledging its contribution to electrostatic behavior certainly helps to understand why experiments related to charge build-up and charge dissipation in dielectrics are

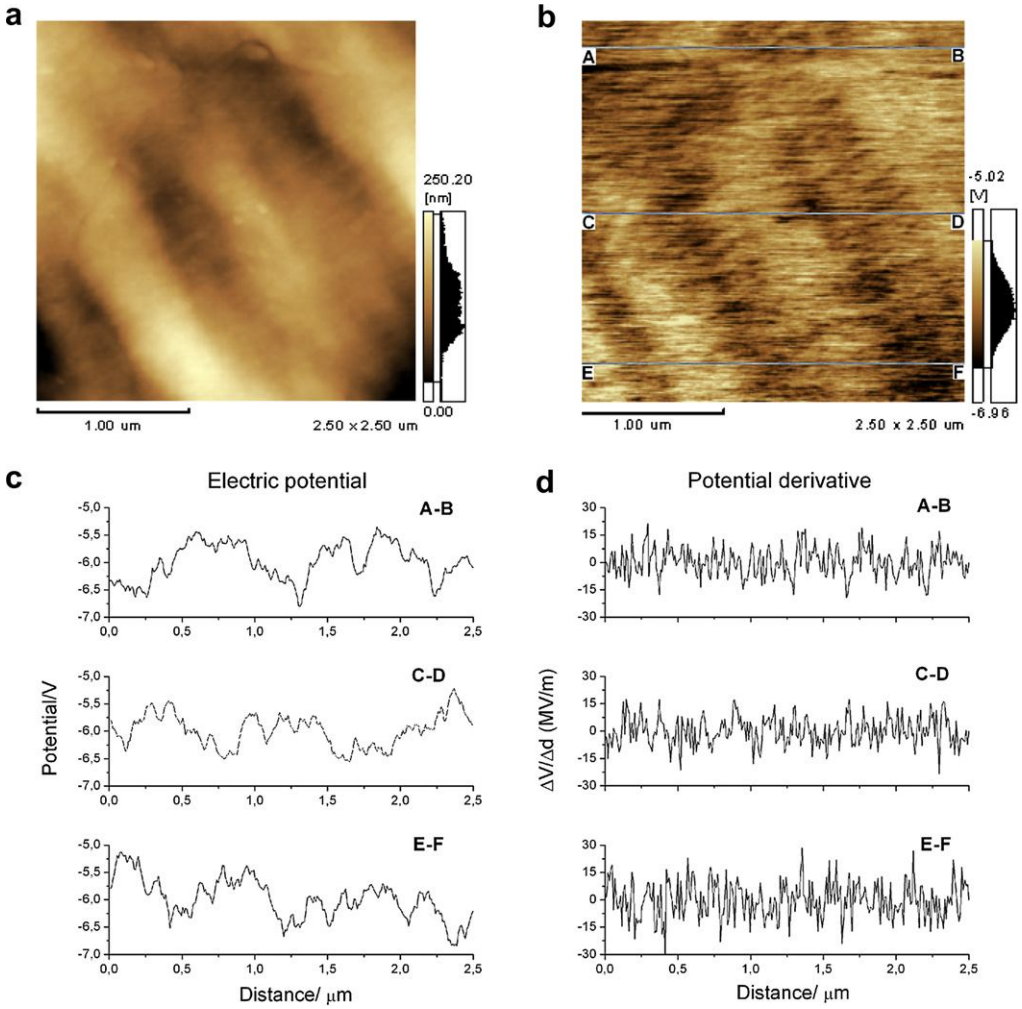

Fig. 11. (a) Topography and (b) electric potential images obtained by KFM on LDPE samples washed with HCl, together with (c) electric potential profiles A–B, C–D and E–F, traced in (b) and the corresponding potential derivative lines, yielding the electric field along the *x*-axis.

hardly reproducible as well as the difficulties to establish consistent triboelectric series [43], added to the persistent discussion on the difference between contact electrification and triboelectrification.

Surface charge concentrations that account for the measured potentials within the range used in this work are very low, *ca.* 0.1–1 charges per square micrometer. Assuming that the surface charge carriers are ions with a 0.01 nm^2 projection area, the area occupied by charge carriers on the surface of a LDPE sample is 1 to 2 parts per billion and the number of excess charge-bearing species per 25 mm^2 pixel in the potential maps may be as low as 2.5×10^7, or 4×10^{-17} mol. Therefore, very small chemical changes as well as very low concentrations of contaminants in the polyethylene surface can account for electrostatic potentials in the range of many tens to hundred volts.

It is thus essential that surface heterogeneity is taken into account and, as far as possible, properly controlled when performing experiments for the study of electric phenomena in dielectrics. In the present work, this was done by taking large numbers of measurements from many individual points in different samples and the successful outcome was the emergence of well-defined patterns for charge dissipation together with the detection of a non-zero equilibrium potential for polyethylene.

The fact that different points on each sample display distinct potential dissipation patterns is a clear indication that dissipation is not mainly due to charge conduction on the surface of the material. Otherwise, all points would be expected to have interdependent dissipation patterns, due to neighboring points exchanging charges through surface conduction up to an equilibrium condition, when zero excess charge would prevail throughout and any excess charges would have migrated to ground.

The negative equilibrium potentials on LDPE can be explained assuming that negative ions are more common than positive ions at LDPE bulk and surfaces at room temperature, other conditions being equal. Absorbed [44] or atmospheric water can contribute $[H(H_2O)_n]^+$ as well as $[OH(H_2O)_n]^-$ ions, among other less common species [45,46]. Specific OH^- adsorption at water–oil and water–air interfaces is well established in the literature [47–49] and an analogous specific adsorption can also be considered in the LDPE-moist/N_2 interface thus accounting for the excess negative potential at equilibrium. A theoretical study on the structural reasons for this behavior was recently published in Ref. [50]. The amount of negative charges on the surface of LDPE is much lower than the value of charge density on the surface of hydrophobic dielectric samples immersed in water (approximately 10^2 charges/μm^2), evidencing that a continuous water layer is not formed on the LDPE surface up to 60% RH.

The negative equilibrium potentials at 1% and 60% RH values are equal within experimental error, quite opposite to the widespread belief that electrostatic charging is always less pronounced under high RH. This also means that the equilibrium potential does not depend on recent exposure of polyethylene to dry or humid air and this may be explained by recalling that sorption in thick polymer specimens is essentially irreversible, due to very slow desorption kinetics [51,52]. Charging state of a thick polymer specimen is thus dependent on contributions from polymer surface and polymer bulk, where the bulk contribution changes very slowly only and thus it is constant within the timespan used in the present experiments. This may be the reason for the Kondo effect described by Schein [53,54] that is the charge exchanged between toner particles and carrier, until the field between them reaches some tens of volts per micrometer. This is called the effective electric field, meaning that toner particles are stabilized at a non-zero potential after contacting the toner and it is the basis for the high density surface state theory of toner electrification. The effective electric field has not yet been associated to any material property [55] and we suggest that it is due to the excess hydroxyl ions (quasi) irreversibly absorbed within the polymer bulk. Microscopic measurements made on LDPE surface shows that the field parallel to the polymer surface reaches 15–30 MV/m, within the range given by Schein for the effective electric field.

The potential decay kinetics can then be related to charge acquisition and dissipation rates at distinct sample surface points. Assuming that atmospheric water is the prevalent sink for ions in this system, the potential change rate is dependent on the rates of water vapor sorption at different spots of LDPE and these should in turn depend on the chemical composition at these points.

This model was used to explain the electric potential build-up and dissipation behavior as the relative humidity is varied in different systems, including silica and aluminum phosphate particles, cellulose, and metallic samples. Silica and aluminum phosphate become more positive or more negative, just by changing the amount of atmospheric humidity within a grounded and shielded environment [36], and isolated metals also acquire electrostatic charge under high humidity [38]. For cellulose samples, rates of charge accumulation and dissipation on samples submitted to an electric field are symmetrical for negative and positive potentials, and they are faster under increased humidity [35].

Ion release by water is dependent upon the electrochemical potential of each water ion that in turn depends on the local potential, according to Eq. (3).

$$\mu_i = \mu_i^{\circ} + \mathrm{RT}\ln a_i + z\mathrm{FV} \tag{3}$$

where i represents H^+ or OH^-. Therefore, H^+ concentration increases under a negative potential and OH^- increases under a positive potential. Ions are thus transferred out of a region with a positive potential to a sink that is the atmosphere and this is faster under high RH, because the rates of adsorption and desorption of water molecules and cluster ions are faster. Beyond, the increase in H^+ and OH^- ions also increases surface conductivity [56].

The difference between the dissipation rates of positive and negative charges evidenced in Figs. 3 and 6 shows that positive excess corona charge decays faster than negative charges and positive charge dissipation is more strongly affected by variation in RH than negative charge dissipation.

This observation is consistent with the excess negative potential observed at equilibrium, and it can also be explained by preferential adsorption of OH^- ions on hydrophobic surfaces that reduces the efficiency of the exchange of negative species with the atmosphere, as compared to positive charges.

Another hypothesis is that faster decay of positive potentials is due to higher cation mobility at the polymer surface, analogous to a Grothuss [57] type of mechanism for ion conduction. However, this kind of mechanism can only be considered if we assume that water molecules on the LDPE surface form a continuous bidimensional network, but this is not possible under the submonolayer coverage conditions used in the present experiments.

5. Conclusions

LDPE surface heterogeneity is revealed by electrostatic potential dissipation rates, equilibrium electrostatic potential and two types of electrical probe mapping microscopy (KFM, EFM). It is assigned to surface chemical and structural heterogeneity of the polymer itself as well as to contaminants in very low concentrations, below detection limits for most surface analytical methods.

Both the dissipation rates and electrostatic equilibrium potentials are explained assuming that negative water cluster ions are adsorbed in LDPE, stronger than the water positive ions. Moreover, negative ions sorbed in the polymer bulk impart a steady charge to

the polymer that has a very large half-life due to the quasi-irreversible characteristics of sorption in polymers.

All the new results presented in this work as well as previous information in the literature are consistent with a model for insulator charging that takes into account the adsorption of ions formed by dissociation of water vapor or adsorbed water molecules. According to this model, atmosphere is an important and probably major source and sink of water ions contributing to electrostatic behavior of dielectric solids.

Acknowledgments

The authors thank Fapesp and CNPq for the financial support and fellowships. This is a contribution from INOMAT, National Institute for Complex Materials, funded by INCT Program (CNPq and Fapesp).

Appendix. Supplementary data

Supplementary data associated with this article can be found, in the online version, at doi:10.1016/j.elstat.2011.05.005.

References

[1] R. Gerhard-Multhaupt, Electrets, third ed., vol. 2, Laplacian Press, Morgan Hill, 1999.
[2] G.M. Sessler, Electrets: recent developments, J. Electrostat. 51 (2001) 137–145.
[3] L.B. Schein, Applied physics – recent progress and continuing puzzles in electrostatics, Science 316 (5831) (2007) 1572–1573.
[4] M.D. Taylor, P.E. Seeker, Industrial Electrostatics: Fundamentals and Measurements. Research Studies Press, Stevenage, 1994.
[5] A. Frenot, I.S. Chronakis, Polymer nanofibers assembled by electrospinning, Current Opinion in Colloid and Interface Science 8 (1) (2003) 64–75.
[6] F. Galembeck, C.A.R. Costa, in: P. Somasundaran, A. Hubbard (Eds.), second ed., Encyclopedia of Surface and Colloid Science, vol. 3 Marcel Dekker, New York, 2006, pp. 1874–1883.
[7] M. Braga, C.A.R. Costa, C.A.P. Leite, F. Galembeck, Scanning electric potential microscopy imaging of polymer latex films: detection of supramolecular domains with non-uniform electrical characteristics, J. Phys.Chem. B. 105 (15) (2001) 3005–3011.
[8] A.J. Keslarek, C.A.R. Costa, F. Galembeck, Latex film morphology and electrical potential pattern dependence on serum components: a scanning probe microscopy study, J. Colloid Interf. Sci. 255 (1) (2002) 107–114.
[9] F. Galembeck, C.A.P. Leite, M.D.V.M. da Silva, A.J. Keslarek, C.A.R. Costa, E. Teixeira-Neto, M.M. Rippel, M. Braga, Polymer electrostatics: detection and speciation of trapped electric charges by electric probe and analytical electron microscopy, Macromol. Symp. 189 (2002) 15–26.
[10] A.H. Cardoso, C.A.P. Leite, F. Galembeck, Latex particle self-assembly and particle microchemical symmetry: PS/HEMA latex particles are intrinsic dipoles, Langmuir 15 (13) (1999) 4447–4453.
[11] O.D. Jefimenko, D.K. Walker, Electrets, Phys. Teach 18 (1980) 651–659.
[12] E. Németh, V. Albrecht, G. Schubert, F. Simon, Polymer tribo-electric charging: dependence on thermodynamic surface properties and relative humidity, J. Electrostat 58 (2003) 3–16.
[13] H.O. Jacobs, H.F. Knapp, A. Stemmer, Surface potential mapping: a qualitative material contrast in SPM, Ultramicroscopy 69 (1) (1997) 39–49.
[14] A.F. Diaz, R.M. Felix-Navarro, A semi-quantitative tribo-electric series for polymeric materials: the influence of chemical structure and properties, J. Electrostat 62 (2004) 277–290.
[15] A. Galembeck, C.A.R. Costa, M.C.V.M. da Silva, E.F. Souza, F. Galembeck, Scanning electric potential microscopy imaging of polymers: electrical charge distribution in dielectrics, Polymer 42 (11) (2001) 4845–4851.
[16] M.D. Hogue, C.R. Buhler, C.I. Calle, T. Matsuyama, W. Luo, E.E. Groop, Insulator-insulator contact charging and its relationship to atmospheric pressure, J. Electrostat 61 (2004) 259–268.
[17] M.D. Hogue, E.R. Mucciolo, C.I. Calle, C.R. Buhler, Two-phase equilibrium model of insulator-insulator contact charging with electrostatic potential, J. Electrostat 63 (2005) 179–188.
[18] M.D. Hogue, E.R. Mucciolo, C.I. Calle, Triboelectric, corona, and induction charging of insulators as a function of pressure, J. Electrostat 65 (2007) 274–279.
[19] D.K. Das-Gupta, Electrical properties of surfaces of polymeric insulators, IEEE T. Electr. Insul 27 (1992) 909–923.
[20] L.S. McCarty, G.M. Whitesides, Electrostatic charging due to separation of ions at interfaces: contact electrification of ionic electrets, Angew. Chem. Int. Edit 47 (12) (2008) 2188–2207.
[21] S.W. Thomas, S.J. Vella, G.K. Kaufman, G.M. Whitesides, Patterns of electrostatic charge and discharge in contact electrification, Angew. Chem. Int. Ed. 47 (35) (2008) 6654–6656.
[22] L.S. McCarty, A. Winkleman, G.M. Whitesides, Ionic electrets: electrostatic charging of surfaces by transferring mobile ions upon contact, J. Am. Chem. Soc. 129 (13) (2007) 4075–4088.
[23] C. Liu, A.J. Bard, Electrostatic electrochemistry at insulators, Nat. Mater. 7 (2008) 505–509.
[24] P.J. Harrop, Dielectrics. Butterworths, London, 1972.
[25] J. Guardiola, V. Rojo, G. Ramos, Influence of particle size, fluidization velocity and relative humidity on fluidized bed electrostatics, J. Electrostat 37 (1996) 1–20.
[26] S.R. Woodhead, D.I. Armour-Chelu, The influence of humidity, temperature and other variables on the electric charging characteristics of particulate aluminium hydroxide in gas–solid pipeline flows, J. Electrostat 58 (2003) 171–183.
[27] K. Das-Gupta, W.F. Schmidt, Electrical properties of surfaces of unirradiated and irradiated polymers in humid environments, IEEE T. Compon. Pack. A 18 (2) (1995) 266–269.
[28] L. Herous, M. Nemamcha, M. Remadnia, L. Dascalescu, Factors that influence the surface potential decay on a thin film of polyethylene terephthalate (PET), J. Electrostat 67 (2009) 198–202.
[29] E. Schrödinger, Über die Leitung der Elektrizität auf der Oberfläche von Isolatoren an feuchter Luft, Ph.D. thesis, University of Wien, Wien, 1910.
[30] R.S. Blacker, A.W. Birley, Electrostatic charge occurrence, significance and measurement, Polym. Test. 10 (4) (1991) 241–262.
[31] R.F. Field, The formation of ionized water films on dielectrics under conditions of high humidity, J. Appl. Phys. 17 (5) (1946) 18–325.
[32] L. Zhengliang, T.B. Xiaotao, J.R. Grace, Electrostatic charging behavior of dielectric particles in a pressurized gas-solid fluidized bed, J. Electrostat 68 (2010) 321–327.
[33] R.F. Gouveia, C.A.R. Costa, F. Galembeck, Electrostatic patterning of a silica surface: a new model for charge build-up on a dielectric solid, J. Phys. Chem. B. 109 (10) (2005) 4631–4637.
[34] R.F. Gouveia, C.A.R. Costa, F. Galembeck, Water vapor adsorption effect on silica surface electrostatic patterning, J. Phys. Chem. C 112 (44) (2008) 17193–17199.
[35] L.C. Soares, S. Bertazzo, T.A.L. Burgo, V. Baldim, F. Galembeck, A new mechanism for the electrostatic charge build-up and dissipation in dielectrics, J. Braz. Chem. Soc. 19 (2) (2008) 277–286.
[36] R.F. Gouveia, F. Galembeck, Electrostatic charging of hydrophilic particles due to water adsorption, J. Am. Chem. Soc. 131 (32) (2009) 11381–11386.
[37] J.S. Bernardes, C.A. Rezende, F. Galembeck, Electrostatic patterns on surfactant coatings change with ambient humidity, J. Phys. Chem. C 114 (44) (2010) 19016–19023.
[38] T.R.D. Ducati, L.H. Simões, F. Galembeck, Charge partitioning at gas/solid interfaces: humidity causes electricity build up on metals, Langmuir 26 (17) (2010) 13763–13766.
[39] C.A. Rezende, R.F. Gouveia, M.A. da Silva, F. Galembeck, Detection of charge distributions in insulator surfaces, J. Phys. Condens. Matter 21 (26) (2009) 263002.
[40] J. Griffiths, Introduction to Electrodynamics, third ed. Prentice Hall, New Jersey, 1999.
[41] A. Baum, T.J. Lewis, R.J. Toomer, Decay of electrical charge on polyethylene films, J. Phys. D Appl. Phys. 10 (4) (1977) 487–497.
[42] J.S. Rigden, Macmillan Encyclopedia of Physics, vol. 1, Simon & Schuster Macmillan, New York, 1996, 353.
[43] J.O. Henniker, Triboelectricity in polymers, Nature 196 (1962) 474.
[44] E. Johansson, K. Bolton, D.N. Theodorou, P.J. Ahlström, Monte Carlo simulations of equilibrium solubilities and structure of water in n-alkanes and polyethylene, J. Chem. Phys. 126 (22) (2007) 22492-1–22492-7.
[45] C.M. Banic, J.V. Iribarne, Equilibrium constants for clustering of neutral molecules about gaseous ions, J. Chem. Phys. 83 (12) (1985) 6432–6448.
[46] V.V. Turov, I.F. Mironyuk, Adsorption layers of water on the surface of hydrophilic, hydrophobic and mixed silicas, Colloid Surf. A 134 (3) (1998) 257–263.
[47] T.W. Healy, D.W. Fuerstenau, The isoelectric point/point-of-zero-charge of interfaces formed by aqueous solutions and nonpolar solids, liquids and gases, J. Colloid Interf. Sci. 309 (1) (2007) 183–188.
[48] K.G. Marinova, R.G. Alargova, N.D. Denkov, O.D. Velev, D.N. Petsev, I.B. Ivanov, R.P. Borwankar, Charging of oil–water interfaces due to spontaneous adsorption of hydroxyl ions, Langmuir 12 (8) (1996) 2045–2051.
[49] J.K. Beattie, A.N. Djerdjev, G.G. Warr, The surface of neat water is basic, Faraday Discuss. 141 (2009) 31–39.
[50] K.N. Kudin, R.J. Car, Why are water–hydrophobic interfaces charged? J. Am. Chem. Soc. 130 (12) (2008) 3915–3919.
[51] A.M. Dorfman, Ya.M. Zolotovitskii, A.M. Lyakhovich, A.E. Chalykh, S.M. Reshetnikov, The desorption of a volatile corrosion inhibitor from polyethylene, Prot. Metals 37 (1) (2001) 9–12.
[52] P.Neogi, Diffusion in Polymers, Marcel Dekker, New York, 1996, pp. 178–181.
[53] L.B. Schein, Recent advances in our understanding of toner charging, J. Electrostat 46 (1999) 29–36.
[54] L.B. Schein, Electric field theory of toner charging, J. Imaging Sci. Technol. 44 (6) (2000) 475–483.
[55] L.B. Schein, Role of technical innovation in the physics of electrophotography, J. Imaging Sci. Technol. 54 (2) (2010) 020201–020209.
[56] W. Bauser, H. Klopffer, H. Rabenhorst, Advance in Static Electricity, vol. 1, Auxilia, Brussels, 1970, 1–9.
[57] N. Agmon, The Grotthuss mechanism, Chem. Phys. Lett. 244 (1995) 456–462.